Real-time aging trajectory prediction using a base model-oriented gradient-correction particle filter for Lithium-ion battery management

Xiaopeng Tang[a], Kailong Liu[b,*], Xin Wang[a], Boyang Liu[a], Furong Gao[a,c,**], W. Dhammika Widanage[b]

[a] *Department of Chemical and Biological Engineering, Hong Kong University of Science and Technology, Clear Water Bay, Kowloon, Hong Kong SAR*
[b] *WMG, The University of Warwick, Coventry CV4 7AL, United Kingdom*
[c] *Guangzhou HKUST Fok Ying Tung Research Institute, Guangzhou 511458, China*

Abstract

Obtaining the information on batteries' future degradation is essential for power scheduling and energy management. The technical challenges arise from the absence of a full battery degradation model and the inevitable local fluctuations of the aging trajectory. In response, an attempt has been made in this paper to derive a model-oriented gradient-correction particle filter (GC-PF) for aging trajectory prediction of Lithium-ion battery management. Specifically, under the framework of typical particle filter, a gradient corrector is first employed for each particle, resulting in the evolution of particle could follow the direction of gradient descent. Then, a model-based regulation is added to the gradient corrector. In this way, the global optimal modeling information suggested by the base model is fully utilized, and the algorithm's sensitivity to the local behaviors could be reduced accordingly. Further, the weighting factors of the local observation and the base model in the gradient correction are both updated online based on the fitness between the base model and the measured trajectories.

*Corresponding author. Address: WMG, The University of Warwick, Coventry CV4 7AL, United Kingdom. Phones: +447477290206. Email: kliu02@qub.ac.uk

**Corresponding author. Address: The Hong Kong University of Science and Technology, Clear Water Bay, Hong Kong SAR. Phone: +852-23587139. Email: kefgao@ust.hk

Email addresses: xtangai@connect.ust.hk (Xiaopeng Tang), kliu02@qub.ac.uk (Kailong Liu), wangx@connect.ust.hk (Xin Wang), bliu@connect.ust.hk (Boyang Liu), kefgao@ust.hk (Furong Gao), Dhammika.Widanalage@warwick.ac.uk (W. Dhammika Widanage)

The proposed algorithm is extensively verified using four different battery data sets. Quantitatively, a root mean square error of the proposed model-oriented GC-PF approach is limited to 1.75% , which is 44% smaller than that of the conventional particle filter. In addition, the consistency of the corresponding predictions when using different size of the training data is also improved by 32%. Due to pure data-driven characteristics, the proposed algorithm can be readily applied in real-time battery aging predictions of energy management.
Keywords: Lithium-ion batteries; Energy management; Gradient Correction; Bayesian Monte Carlo; Aging trajectory prediction; State-of-health

1. Introduction

The inevitable battery degradation is a key factor that influences the battery efficiency regarding the applications of energy managements [1], thermal managements [2], charging managements [3], balancing managements [4], and economic managements [5]. For instance, an aged battery could have a 20% reduction in its available capacity and 100% increase in its internal resistance for electrical vehicle (EV) applications. In some special cases, degradation can even lead to battery failure and safety issues [6]. In response, extensive studies on the estimations of real-time battery state of health (SOH) have been carried out [7, 8]. However, only using current SOH information is not sufficient for power scheduling and energy management because users generally want to know how many remaining life can a battery still own. This information regarding the remaining useful life is critical for reducing the users' anxiety about the battery lifespan and safety [9, 10]. Further, the prediction of battery capacity degradation can also benefit the optimization of battery operations and the improvement of energy systems' efficiency and reliability [11]. Therefore, it is also imperative to predict the battery's future capacity aging behaviors for efficient energy management.

One most straightforward solution to obtain the degradation trajectory of battery capacity is through conducting the direct experiments under a specific

load condition. However, this solution generally requires quite a long experimental time of several months or even years [12]. The batteries after experiments would be largely degraded and no longer be used. Therefore, this solution is commonly adopted in the lab to provide referenced aging trajectories rather than applied in real-time applications.

To achieve effective online predictions of battery aging, the first thing is to obtain the existing degradation trajectories. After that, various algorithms are employed to extract the tendency of battery degradation over time, so that the future predictions can be made through reasonably extending the battery aging tendency. Such algorithms could be categorized into three categories, namely, time-series based approach, data-fitting based approach, and filter based approach.

For the time-series based prediction approaches, the battery's SOH after future M steps degradation (SOH_{k+M}), is assumed to have some underlying relations with the historical SOHs obtained from the previous N steps ($SOH_{k-N+1:k}$) [13]. To capture these underlying relations, various artificial intelligence technologies such as neural network [14], support vector machine [15], and relevant vector machine [16] have been successfully adopted. One obvious benefit of using this kind of method is that the time-series information of battery aging tendency can be captured after learning process, and an accurate result can be generally achieved for the single-step prediction. However, due to the error accumulation, the accuracy of long-term multi-step predictions will inevitably decrease.

For the data-fitting based prediction approaches, after collecting the battery historical aging data, the underlying mapping between battery SOH and the corresponding time (or cycle number) is captured by fitting the data into a reasonable degradation model. After that, the battery degradation level at various timescale could be predicted through using the established model. One effective model type here is the physics-based models that use several partial differential equations to directly explain battery aging behaviors [17, 18]. Although attractive electrochemical dynamics of battery aging can be analysed in

the simulation environment, these physics models are generally highly memory-consuming and complex to be fitted, making them overly expensive for real-time aging trajectory predictions [19]. As an alternative, simple but effective empirical models such as the single exponential model [20], dual-exponential model [21], linear model [22] or polynomial model [23] are generally adopted. Due to the characteristics of straightforward and easy to implement, the empirical model fitting-based predictions are widely used in battery management systems (BMS). However, it should be noted that a simplified empirical model tend to be noise-sensitive, especially when the training data is limited.

For the filter based prediction approaches, the parameters in an aging model are treated as state variables and identified online through state observers or filters. In comparison with the empirical prediction based approach, the noise-sensitivity of this type of algorithms is reduced with the help of advanced observers or filters. Further, the filtering based approaches are more suitable for real-time applications as the corresponding calculations can be carried out recursively. In light of this, filter based predictor is regarded as one of the most promising algorithm for predicting the battery degradation dynamics. Commonly used filtering algorithms include the Luenberger observer [24], Kalman filter-based algorithms [25], and particle filter (PF)-based algorithms [26]. Among these algorithms, PF is featured as its superiorities of solving nonlinear and non-Gaussian problems, and has been widely adopted in health prognosis [27]. However, similar to most of the existed observers, the filtering results of PF are largely affected by the initial value, and they would also be more sensitive to the new data than the historical data.

Based on the above analyses, predicting battery aging trajectory is technically challenging due to at least the following two reasons: First, battery degradation is a complex nonlinear process with coupled physical and chemical reactions [28]. A full model describing this process is difficult to obtain and computational complex, while the local aging tendency extracted from the partial historical data may fail to reflect the whole trajectory of long-term battery degradation if a simplified empirical model is selected. Meanwhile, the data

collected for the battery aging trajectory prediction is easy to be polluted by noise in daily applications. For instance, considerable noise may come from cost-effective sensors in the BMS [29] and uncontrollable climate changes over time [30]. This situation is quite different from the cases that adopt the accurate lab-operations [31]. When identifying a nonlinear model with limited training data and considerable noise, it is generally difficult to ensure fitting accuracy. With the presence of above two problems, the predicted aging trajectories would change significantly under the cases of using different size of the training data. From the user's perspective, a trembling prediction result could increase the anxiety on battery lifespan, which requires to be prohibited.

Driven by the purpose to enhance the performance of battery aging trajectory prediction, a base model-oriented gradient-correction particle filter (GC-PF) is proposed in this study. Specifically, the evolution of each particle within the framework of PF is enhanced by a gradient-based estimator, bringing the benefits to improve the particles' tracking performance. Besides, a model-based regularization is also proposed to force the local identification result to well follow the global result, further helping to reduce the algorithm sensitivity to the local behavior of the aging trajectories. Finally, based upon four different battery aging data sets, the prediction performance of our proposed algorithm is investigated and compared with two other benchmarks. To evaluate the prediction consistency under different size of training data, a new criterion is also adopted. This is a promising application by using model regularization technique together with the improved PF to handle battery aging trajectory prediction problem. Obviously, due to the mechanism-free properties, this proposed GC-PF algorithm can be easily extended to other battery types for aging trajectory prediction.

The remainder of this paper is organized as follows: Section 2 specifies the utilized battery aging data sets. Then the elaborations of fundamentals behind classical particle filter, enhanced gradient correction method, and the proposed GC-PF algorithm are presented in Section 3. Section 4 first describes the other two benchmarks and the criteria for algorithm evaluation, followed by the in-

depth analyses of the experimental results. Finally, Section 5 concludes this study.

2. Experimental platform

In this paper, four battery aging data sets are used to verify the proposed method and each set contains the cyclic aging data of two battery cells. The data sets of SONYVTC5, FST2500, and FST2000 batteries are collected in the Guangzhou HKUST Fok Ying Tung Research Institute. Additionally, a widely used aging data benchmark provided by NASA (see [32] for details) is also selected to verify the proposed method.

Specifically, the UPower battery tester, as described in [33], is applied for collecting data from SONYVTC5 and FST2500 batteries. Another Sunway BTS4008 battery tester with the detailed description in [34], is adopted to collect the data from FST2000 batteries. In each operational cycle of all these three batteries, the constant-current constant-voltage (CCCV) profile [35, 36] is first used to fully charge cell, followed by a constant-current (CC) pattern to fully discharge cell during the cyclic aging process.

All the corresponding current and voltage data are continuously collected during cyclic aging tests. Then the discharging capacity is calculated by integrating the current over each cycle. It should be noted that all these tests are carried out under the room temperature without using precise temperature control, bringing more challenges for the adopted algorithms to take the effects of these measured noises into account. Other details of these data sets regarding the rated capacity, current rates, cut-off current, cut-off voltages, and testing cycles are summarized in Table 1.

3. Methodology

In this section, the typical particle filter (PF)-based aging trajectory algorithm is first described with the purpose of comparison and motivating other

Table 1: Description of the selected data sets.

Battery type	FST2500		SONYVTC5		FST2000		NASA	
	#01	#02	#01	#02	#01	#02	#05	#06
Rated capacity (mAh)	2500	2500	2500	2500	2000	2000	2000	2000
Current rate (Chg/Dchg)	0.2C/0.2C	0.4C/0.4C	1C/1C	1C/1C	1C/1C	1C/1C	0.75C/1C	0.75C/1C
Cut-off current	0.05C	0.05C	0.05C	0.05C	0.05C	0.05C	0.01C	0.01C
Cut-off voltage: Chg	4.2V	4.2V	4.2V	4.2V	4.2V	4.2V	4.2V	4.2V
Cut-off voltage: Dchg	2.75V	2.75V	2.75V	2.75V	2.75V	2.75V	2.7V	2.5V

algorithms. Then the innovate state estimator based on the enhanced gradient-corrector is elaborated in details.

3.1. Conventional PF-based aging trajectory prediction

From [33], as the battery capacity $C_n(k)$ at the discrete-time step k is available, the battery state of health (SOH) could be defined as:

$$SOH(k) = C_n(k)/C_n(0) \tag{1}$$

where $C_n(0)$ represents the capacity calibrated at the beginning of battery's service life, and $C_n(k)$ stands for the real capacity that is sampled at each battery operating cycle.

Given a set of aging data, the SOH can be modeled as a function of time or cycle number. Motivated by [37, 38, 39], a generalized polynomial equation with the following form could be adopted to depict the underlying relation between battery SOH and the cycle number k as:

$$SOH(k) = \alpha_1 \cdot k^{\alpha_2} + \alpha_3 \tag{2}$$

where $\boldsymbol{\alpha} = [\alpha_1, \alpha_2, \alpha_3]$ represent the model parameters that require to be determined. More details regarding the effectiveness of this type of polynomial equation has been proven in [38].

To implement the parameter identification under the framework of PF, the evolution of $\boldsymbol{\alpha}$ should be first formulated as:

$$\boldsymbol{\alpha}_k = \boldsymbol{\alpha}_{k-1} + \boldsymbol{\omega}_k \tag{3}$$

where $\boldsymbol{\omega} = [\omega_1, \omega_2, \omega_3]$ are zero-mean Gaussian noises, with standard deviation $\boldsymbol{\sigma} = [\sigma_1, \sigma_2, \sigma_3]$, respectively.

The SOH observation equation can be formulated as:

$$SOH(k) = y_k = \alpha_{1,k} \cdot k^{\alpha_{2,k}} + \alpha_{3,k} + \nu_k \tag{4}$$

where ν is a zero-mean Gaussian noise, with standard deviation equal to σ_ν, and $\alpha_{i,k}$ for $i \in [1, 3]$ is the identified α_i at the kth cycle number.

It should be noted that the initial $\boldsymbol{\alpha}_0$ could significantly affect the algorithm performance. An effective engineering solution is to offline identify (2) with the battery degradation data provided by the datasheet or the existing historical data that covers the full SOH range. To simplify the notations, the offline identified model using the existing battery data is labelled as base model, and the identified model parameter $\boldsymbol{\alpha}_B$ is used to set $\boldsymbol{\alpha}_0$ as:

$$\boldsymbol{\alpha}_0 = \boldsymbol{\alpha}_B \tag{5}$$

When implementing the PF with (3) and (4), one key step is to draw N_s groups of $\boldsymbol{\alpha}$ (also known as particles) from $P(\boldsymbol{\alpha}_k|\boldsymbol{\alpha}_{k-1})$ following (3). Then, for each particle j, the corresponding SOH can be calculated as:

$$y_k^j = \alpha_{1,k}^j \cdot k^{\alpha_{2,k}^j} + \alpha_{3,k}^j \tag{6}$$

Then, the weight associated with particle $\boldsymbol{\alpha}_k^j$ at the kth cycle number could be calculated by [40]:

$$w_k^j = w_{k-1}^j \cdot P\left(y_k|\boldsymbol{\alpha}_k^j\right) = w_{k-1}^j \cdot \frac{1}{\sqrt{2\pi}\sigma_\nu} \exp\left(-\frac{\left(y_k - y_k^j\right)^2}{2\sigma_\nu^2}\right) \tag{7}$$

and then normalized as:

$$w_k^j \leftarrow w_k^j / \sum_{j=1}^{N_s} w_k^j \tag{8}$$

The estimation of $\boldsymbol{\alpha}$ can be given as the weighted summation of each particle as:

$$\hat{\boldsymbol{\alpha}}_k = \sum_{j=1}^{N_s} w_k^j \cdot \boldsymbol{\alpha}_k^j \tag{9}$$

Similarly, the h-step prediction of the aging trajectory can also be obtained by the weighted summation of the prediction generated from each particle [21]:

$$\hat{y}_{k+h} = \sum_{j=1}^{N_s} w_k^j \cdot y_{k+h}^j \tag{10}$$

In order to reduce the particle degradation problem, the following three-step resampling technique is adopted [41].

- for $i = 1, 2, \cdots, N_s$, generating the uniformly distributed random numbers $u_i \in U(0, 1)$.
- after resampling, the i^{th} particle in the new particle set should be equal to the j^{th} particle in the original set under the case of:

$$\sum_{n=1}^{n=j-1} w_k^j < u_i \leq \sum_{n=1}^{n=j} w_k^j \tag{11}$$

- resetting the weight of each particle in the resampled particle set as $1/N_s$.

For the above mentioned process, detailed resampling approach is summarized in Table 2 to guarantee the computational efficiency [27]. Noting that the battery aging could generally take several years, while the algorithm's computational time is only about a few seconds. In this concern, the resampling is carried out at each sampling step in this study.

Table 2: Detailed resampling approach

Function Resample($\boldsymbol{\alpha}_k^{1:N_s}, w_k^{1:N_s}$)

for $i = 1 : N_s$ **do**
  Generate: $u_i \in U(0, 1)$;
  $w_{sum} = 0$;
  for $j = 1 : N_s$ **do**
    $w_{sum} = w_{sum} + w_k^j$;
    if $w_{sum} \geq u_i$ **then**
      $\boldsymbol{\beta}_k^i \leftarrow \boldsymbol{\alpha}_k^j$;
      break;
return $\boldsymbol{\beta}_k^{1:N_s}$;

3.2. Enhanced gradient-corrector

In this subsection, an enhanced gradient-correction (GC)-based state estimator is designed. This estimator is then used together with the PF to improve the performance of battery aging trajectory prediction. For completeness, the following descriptions start with the conventional gradient correction method accordingly.

3.2.1. Batch gradient correction method

In order to determine $\boldsymbol{\alpha}$ in (2) with a batch GC method, it is necessary to seek the $\boldsymbol{\alpha}$ that can minimize the following cost function at k as:

$$J(\boldsymbol{\alpha}, k) = \sum_{n=1}^{n=k} ||y_n - (\alpha_1 \cdot n^{\alpha_2} + \alpha_3)||_2^2 \tag{12}$$

where $|| \cdot ||_2^2$ represents the 2-norm.

Then, (12) can be solved by repeating (13) as [42]:

$$\boldsymbol{\alpha} \leftarrow \boldsymbol{\alpha} - \boldsymbol{\eta} \cdot \nabla_{\boldsymbol{\alpha}} J(\boldsymbol{\alpha}, k) \tag{13}$$

where $\boldsymbol{\eta} = [\eta_1, \eta_2, \eta_3]$ stands for the learning rates, and $\nabla_{\boldsymbol{\alpha}}$ is the gradient operator for $\boldsymbol{\alpha}$:

$$\nabla_{\boldsymbol{\alpha}} J(\boldsymbol{\alpha}, k) = \left[\frac{\partial J(\boldsymbol{\alpha}, k)}{\partial \alpha_1}, \frac{\partial J(\boldsymbol{\alpha}, k)}{\partial \alpha_2}, \frac{\partial J(\boldsymbol{\alpha}, k)}{\partial \alpha_3} \right] \tag{14}$$

This iteration would stop as the obtained gradient becomes smaller than a predefined threshold or the maximum number of iterations is reached.

3.2.2. Enhanced gradient correction method

It should be noted that a GC algorithm based on (12) has two limitations when using it to handle the lifespan prediction problem: First, due to the requirements of storing the historical data from 1st to kth cycle number, the complexity of solving (12) becomes larger with the increase of k. Second, at the kth cycle number, the optimal solution of (12) is obtained based on the data collected from 1 to k. Due to the simplified structure of the empirical model and the inevitable measurement noise in real-time applications, this optimal solution may fail to capture the true degradation tendency of the entire battery lifespan.

Driven by the purpose to address the first problem, at each kth cycle number, the following cost function would be adopted as an alternative:

$$J_k^S(\boldsymbol{\alpha}_k, k) = ||y_k - (\alpha_{1,k} \cdot k^{\alpha_{2,k}} + \alpha_{3,k})||_2^2 \tag{15}$$

Based on this cost function, a new GC-based solution is conducted as:

$$\boldsymbol{\alpha}_k = \boldsymbol{\alpha}_{k-1} - \boldsymbol{\eta} \cdot \nabla_{\boldsymbol{\alpha}} J_k^S(\boldsymbol{\alpha}_{k-1}, k) \tag{16}$$

Following this way, the update would be conducted at each sampling step through only using the information collected at this step, further helping to reduce the corresponding computational complexity.

After that, an attempt has been made through using a novel model-based regularization to address the second issue. The key idea is to use the existing

knowledge of $\boldsymbol{\alpha}_B$ in the entire training process, rather than just for parameter initialization. In details, the cost function in (15) would be enhanced by adding a penalty under the condition of the identified α_i is far away from the referenced $\alpha_{B,i}$:

$$J_k^B(\boldsymbol{\alpha}_k, k) = (1-\lambda_k) \cdot ||y_k - [\alpha_{1,k} \cdot k^{\alpha_{2,k}} + \alpha_{3,k}]||_2^2 + \lambda_k \cdot \left|\left| \left(\frac{\partial y_k}{\alpha_{1,k}}, \frac{\partial y_k}{\alpha_{2,k}}, \frac{\partial y_k}{\alpha_{3,k}} \right) \cdot (\boldsymbol{\alpha}_k - \boldsymbol{\alpha}_B) \right|\right|_2^2 \tag{17}$$

where $\lambda_k \in [0,1]$ represents the weighting factor at k. It can be seen that there exists two parts within the (17). With the same form as (15), the first part is used to describe the deviation between the predicted output and the online collected SOH information. The second part mainly describes the deviation between $\boldsymbol{\alpha}_k$ and $\boldsymbol{\alpha}_B$. Noting that the level of magnitude of α_i in (2) could be different, one partial differential term is adopted to describe the sensitiveness of corresponding parameters.

When the SOH calculated from the base model gets close to the measurement, it is better to keep $\boldsymbol{\alpha}$ becoming close to the existed $\boldsymbol{\alpha}_B$ that represents the global tendency of battery degradation. However, the priority should be shifted into the online measurement if there exists large difference between the SOH from base model and measurement. In light of these considerations, the following heuristic method is adopted to determine λ at time k as:

$$\lambda_k = c \cdot \lambda_{k-1} + (1-c) \cdot \max\left\{0, 1 - \frac{|y_k - y_{B,k}|}{\delta}\right\} \tag{18}$$

where δ represents a threshold to reflect the credibility of base model, c stands for the filtering factor, and $y_{B,k}$ is the battery SOH calculated with the base model as:

$$y_{B,k} = \alpha_{B,1} \cdot k^{\alpha_{B,2}} + \alpha_{B,3} \tag{19}$$

Then, the GC-updating law for $\boldsymbol{\alpha}$ finally becomes the following equation as:

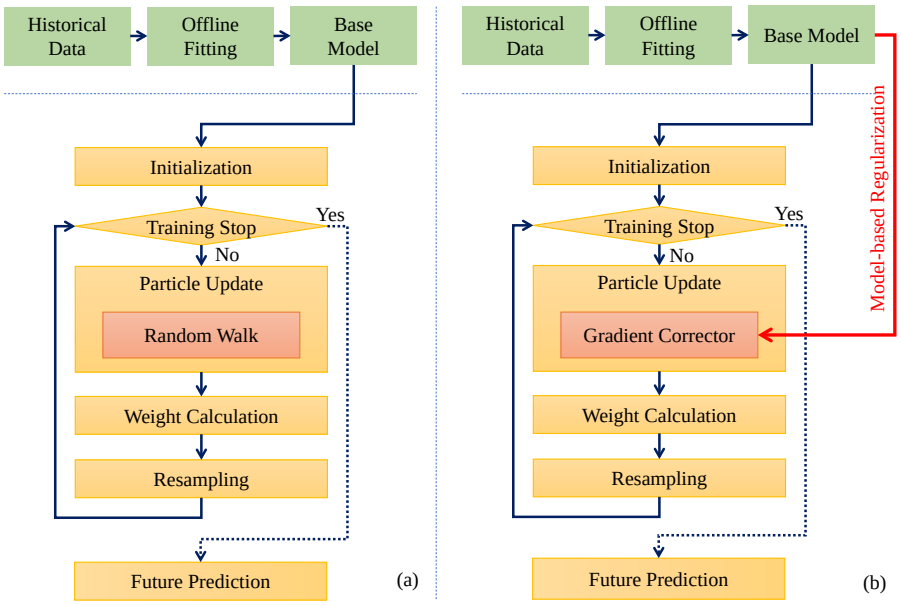

Figure 1: Compassion between the proposed algorithm and the conventional PF. (a): Conventional PF; (b): Proposed GC-PF.

$$\boldsymbol{\alpha}_k = \boldsymbol{\alpha}_{k-1} - \boldsymbol{\eta} \cdot \nabla_{\boldsymbol{\alpha}} J_k^B(\boldsymbol{\alpha}_{k-1}, k) \tag{20}$$

3.3. Proposed GC-PF algorithm

Given the enhanced GC as well as the PF algorithms, the innovate GC-PF algorithm could be formulated for battery aging prediction. A systematic diagram describing the proposed algorithm is shown in Fig. 1, together with that of the conventional PF for comparison. Specifically, the proposed algorithm remains the same framework as the conventional PF that has been mentioned in subsection 3.1. However, the proposed GC-PF algorithm will utilize the GC method on each particle before calculating the corresponding weight. According to this improvement, the evolution of $\boldsymbol{\alpha}$ is no longer a random walk as described in (3). Instead, the particles would move towards a more reasonable direction suggested by the gradient descent, leading to a better tracking capability. In addition, the base model containing the global information is not only used for

parameter initialization, but also incorporated in the gradient corrector throughout the entire training process. Consequently, both the local dynamics of aging trajectory and the global behavior of battery degradation could be taken into account.

Table 3 illustrates the detailed implementation process of proposed GC-PF algorithm. The performance of this algorithm will be experimentally evaluated in Section 4.

4. Experimental Verification

In this section, the effectiveness of the proposed method is extensively verified through experiments. To better illustrate the results, benchmarking algorithms for comparison are first introduced in Section 4.1, followed by the parameter configurations in Section 4.2 and the experimental results in Section 4.3.

4.1. Benchmarks and criteria for algorithm evaluation

In this paper, two benchmarking algorithms are designed. First, the conventional PF is selected as the benchmarking algorithm 1 because it has the similar fundamental structure as the proposed GC-PF. Second, to indicate the best fitting result of (2) under the specific noise conditions, a benchmarking algorithm 2 is adopted. For this algorithm, through employing the offline nonlinear fitting algorithms provided in MATLAB [43], the battery degradation model would be identified based on the full aging data.

Two common criteria, namely, the Root-Mean-Squared-Error (RMSE), and the Maximum-Absolute-Error (MxAE), are used to evaluate the accuracy of these algorithms. Their definitions are provided in equations (21) and (22), respectively [44].

$$\mathrm{RMSE} = \sqrt{\frac{1}{h}\sum_{j=1}^{j=h}\left(\hat{y}_{l+j} - y_{l+j}\right)^2} \tag{21}$$

Table 3: Proposed GC-PF algorithm

Algorithm 1: GC-PF algorithm

Input: Collected SOH from time 1 to l: $y_{1:l}$

Output: h-steps prediction of future SOH: $\hat{y}_{l+1:l+h}$

Initialize: Base model parameters: $\boldsymbol{\alpha}_B$;

Model parameters: $\boldsymbol{\alpha}_0^j = \boldsymbol{\alpha}_B$, for $j = 1 : N_s$;

Particle number: N_s;

Learning rate: $\boldsymbol{\eta}$;

Initial weighting factor for GC: λ_0;

Standard deviation of $\boldsymbol{\omega}$: $\boldsymbol{\sigma}$;

Standard deviation of ν: σ_ν;

Initial particle weight: $w_j = 1/N_s$, for $j = 1 : N_s$;

Filtering factor for λ: c;

for $k = 1 : l$ **do** `// For each sampling step`

- $y_{B,k} = \alpha_{B,1} \cdot k^{\alpha_{B,2}} + \alpha_{B,3}$;
- $\lambda_k = c \cdot \lambda_{k-1} + (1 - c) \cdot \max\left\{0, 1 - |y_k - y_{B,k}| \cdot \delta^{-1}\right\}$;
- **for** $j = 1 : N_s$ **do** `// For each particle`
  - `// PF-based particle update`
  - $\boldsymbol{\alpha}_k^j = \boldsymbol{\alpha}_{k-1}^j + \boldsymbol{\omega}_k$;
  - `// GC-based particle update`
  - $y_k^j = \alpha_{1,k}^j \cdot k^{\alpha_{2,k}^j} + \alpha_{3,k}^j$;
  - $J_k^B = (1 - \lambda_k) \left|\left| y_k - y_k^j \right|\right|_2^2 + \lambda_k \left|\left| \nabla_{\boldsymbol{\alpha}} \left(y_k^j \right) (\boldsymbol{\alpha}_k - \boldsymbol{\alpha}_B) \right|\right|_2^2$;
  - $\boldsymbol{\alpha}_k^j \leftarrow \boldsymbol{\alpha}_k^j - \boldsymbol{\eta} \cdot \nabla_{\boldsymbol{\alpha}} J_k^B$;
  - `// Particle weight calculation`
  - $y_k^j = \alpha_{1,k}^j \cdot k^{\alpha_{2,k}^j} + \alpha_{3,k}^j$;
  - $w_k^j = w_{k-1}^j \cdot \frac{1}{\sqrt{2\pi}\sigma_\nu} \exp\left(-\frac{\left(y_k - y_k^j\right)^2}{2\sigma_\nu^2} \right)$;
- `// Weight normalization`
- $w_k^j \leftarrow w_k^j / \sum_{j=1}^{N_s} w_k^j$;
- `// Resampling`
- $\boldsymbol{\alpha}_k^{1:N_s} \leftarrow \text{Resample}(\boldsymbol{\alpha}_k^{1:N_s}, w_k^{1:N_s})$;
- $w_k^{1:N_s} = 1/N_s$;

for $k = 1 : h$ **do** `// Future predictions`

- $y_{l+k}^j = \alpha_{1,k}^j \cdot (l + k)^{\alpha_{2,k}^j} + \alpha_{3,k}^j$;
- $\hat{y}_{l+k} = \sum_{j=1}^{N_s} w_k^j \cdot y_{l+k}^j$;

return $\hat{y}_{l+1:l+h}$;

$$\mathrm{MxAE} = \max_{j\in[1,h]} |\hat{y}_{l+j} - y_{l+j}| \tag{22}$$

In addition, to evaluate the consistency of predictions under the cases of using the different sizes of training dataset, a new criterion, the Standard-Deviation of predictions at the end of test (SDE), is proposed in this study. This criterion can be defined by the following way: when using the same data set, M predictions can be made with different size of training data, denoted as $[l_1, l_2, \cdots, l_M]$. Accordingly, the predicted SOH at cycle L can be denoted as $[\hat{y}_{l_1+h_1}, \hat{y}_{l_2+h_2}, \cdots, \hat{y}_{l_M+h_M}]$, where $h_j + l_j = L$ holds for $\forall j \in [1, M]$. Then, the SDE can be calculated by:

$$\mathrm{SDE} = \sqrt{\frac{\sum_{j=1}^{j=M} \left(\hat{y}_{l_j+h_j} - \bar{y}_L\right)^2}{M-1}} \tag{23}$$

where $\bar{y}_L$ is the average SOH of these M predictions. The smaller the SDE, the prediction performance of algorithm is less sensitive to the size of training data. Due to the second benchmark uses the full range SOH data, the SDE is only applied to the proposed GC-PF and conventional PF algorithms.

4.2. Algorithm configurations

Before presenting the detailed prediction results, corresponding algorithm configurations are introduced first to ensure the repeatability. For each data set, the base model is built through using the data from the first cell, and then the aging trajectory prediction is carried out on the second cell.

The base model is identified by the offline least-square method under the MATLAB nonlinear fitting toolbox, and the particles for both the proposed algorithm and the conventional PF algorithm are initialized by the parameters of base model. Here the particle number and the standard deviation for all related algorithms are set as 100 and 0.001, respectively. For our proposed GC-PF algorithm, the initial weighting factor λ_0 is set as 1. That is, we fully trust the base model when no measurements are available. The filtering factor c is

selected as 0.1. The standard deviation of $\boldsymbol{\omega}$ and the learning rate $\boldsymbol{\eta}$ would vary with the noise and the size of data sets. Detailed configurations of the proposed and benchmarking algorithms are listed in Table 4. Specifically, we selected the same $\boldsymbol{\omega}$ for the proposed algorithm and conventional PF to ensure a fair comparison. For the first three groups of batteries (FST2500, SONYVTC5, and FST2000), the battery aging trajectories are predicted using 10%, 20%, 30% and 40% of the total data. For the NASA data set, there only exists 168 testing results for each battery, which makes 10% of total data become too limited. Therefore, the predictions are carried out after using the first 20%, 30%, 40% and 50% of total data to train models.

Table 4: Configurations of the proposed algorithm and conventional PF

Battery	Proposed & Conventional PF			Proposed		
	ω_1	ω_2	ω_3	η_1	η_2	η_3
FST2500	$3 \cdot 10^{-7}$	10^{-3}	10^{-3}	$3 \cdot 10^{-8}$	10^{-2}	10^{-2}
SONYVTC5	$3 \cdot 10^{-6}$	10^{-3}	10^{-3}	$3 \cdot 10^{-5}$	10^{-2}	10^{-2}
FST2000	10^{-5}	10^{-3}	10^{-3}	10^{-6}	10^{-2}	10^{-2}
NASA	10^{-5}	10^{-3}	10^{-3}	10^{-5}	10^{-2}	10^{-2}

4.3. Experimental results

The experimental results of the utilized four batteries are illustrated in Fig. 2 $\sim$ Fig 5, respectively. Here "Dat Sz" represents the corresponding training data size. The RMSE, MxAE and SDE of both the proposed and the benchmarking algorithms are also provided in Table 5. According to these prediction results, several observations could be made.

First, for the cases of providing sufficient training data and a relatively small measurement noise, both the proposed GC-PF and the conventional PF algorithms are effective for predicting the battery aging trajectory. Taking FST2500 battery data set as an example, both the proposed GC-PF and the benchmark 1 algorithms can provide reliable performance for such cases. Quant-

Table 5: Prediction performance of the proposed and benchmarking algorithm

Battery Type	Training data size	Proposed				Benchmark 1				Benchmark 2
		10%	20%	30%	40%	10%	20%	30%	40%	100%
FST2500	RMSE (%)	0.99	1.22	1.05	1.14	2.73	1.15	3.10	1.05	0.76
	MxAE (%)	5.03	6.05	4.44	5.19	5.29	5.78	10.14	4.48	3.89
	SDE (%)	0.67				4.32				-
SONYVTC5	RMSE (%)	1.19	1.06	1.16	0.95	1.2	1.45	1.95	2.62	0.91
	MxAE (%)	2.94	3.02	2.79	2.09	2.98	3.71	4.24	5.21	2.22
	SDE (%)	0.99				2.18				-
FST2000	RMSE (%)	1.18	1.24	1.86	1.60	1.21	1.26	1.96	3.10	1.12
	MxAE (%)	2.65	2.75	3.73	3.27	3.01	2.79	3.85	5.18	3.02
	SDE (%)	0.62				1.92				-
Battery type	Training data size	20%	30%	40%	50%	20%	30%	40%	50%	100%
NASA	RMSE (%)	1.66	3.71	1.75	0.98	1.62	4.12	1.97	1.32	1.62
	MxAE (%)	4.74	5.19	2.71	4.56	5.1	5.69	2.92	4.6	4.77
	SDE (%)	1.99				2.93				-

itatively, the RMSE of all predictions is limited within 1.5% when the training data set covers 40% of the battery lifespan.

Second, under the conditions of using 10% data for training purpose, the RMSEs of conventional PF algorithm may become even better than the cases of 20% to 40%. This is mainly due to the fact that PF highly relies on the initialization when the training data is limited, and the initial $\boldsymbol{\alpha}_0$ for the first three batteries are all suitable (this could be verified by checking Fig. 2-(a) $\sim$ Fig. 4-(a)). The RMSE of the predictions with first 10% of the data can be limited within 2.73%. For the SONYVTC5 and FST2000 batteries whose aging curves are close to linear, the RMSE can become even better than 1.21%.

Third, the conventional PF tends to track the local behaviors of the measured aging trajectories. These "local behaviors" represent the local degradation rate, the disturbances in the aging curves (caused by the measurement noise and the ambient temperature change), and their combinations. To be specific, it can be seen from Fig. 2 that the battery degradation rate increases over time. When predicting the aging trajectory after using the first 30% data (108 cycles) for training purpose, the PF tends to use the local battery degradation rate around the 108th cycle to predict the future remaining trajectory. As a result,

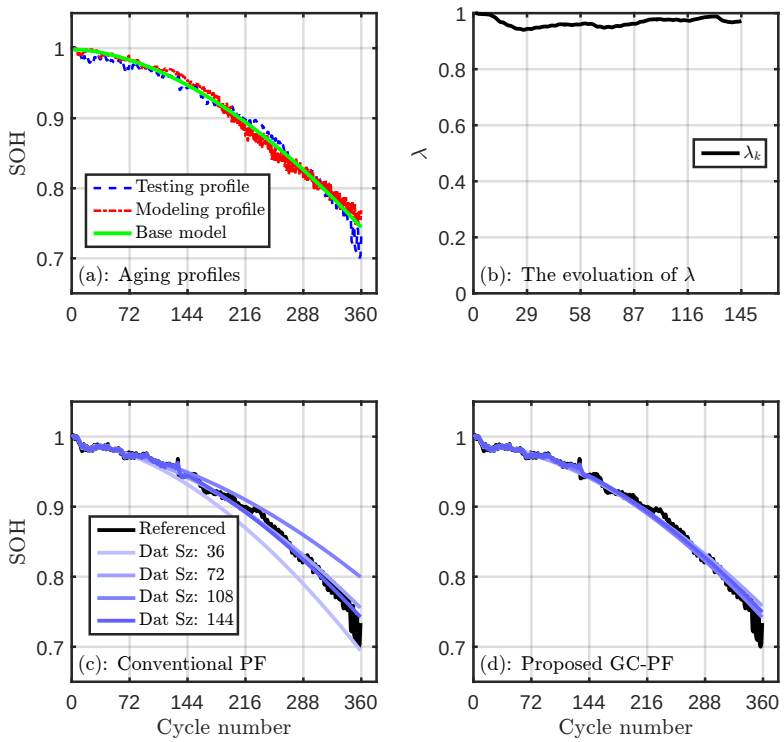

Figure 2: Experimental results using FST2500 batteries. (a): Aging profiles of modeling and testing profiles; (b): The evolution of λ over time; (c): Predicted aging trajectories using conventional PF; and (d): Predicted aging trajectories using the proposed GC-PF.

the predicted aging trajectory becomes significantly higher than the referenced curve. The RMSE of this prediction is 3.10%, and the MxAE exceeds 10%. An example regarding the influence of noise can be found in Fig. 3. The aging trajectory of the testing profile presents a rapid decrease around the 160th cycle. And according to Fig. 3-(c), the predicted aging trajectory through using 40% of the aging data (160 cycles) is indeed lower than the referenced curve. Here, the RMSE also exceeds 3%. Fig. 4 provides an example of the effects of both noise and degradation rate variation. It is straightforward to see that this data set is first heavily polluted by noise. In addition, the local degradation rate from the 230th cycle to 320th cycle is faster than that suggested by the base model. As a result, the predicted aging curve using 40% of the aging data (320

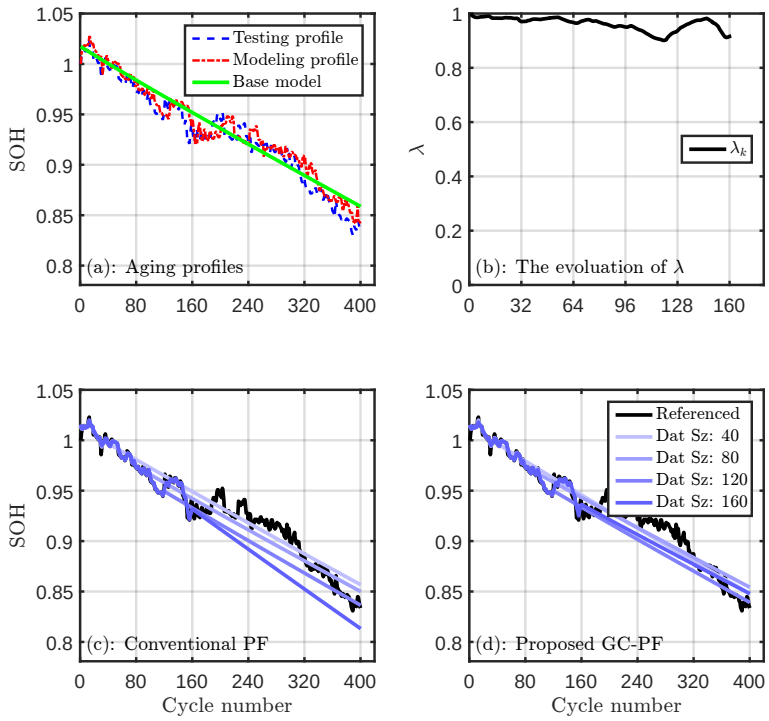

Figure 3: Experimental results using FST2000 batteries. (a): Aging profiles of modeling and testing profiles; (b): The evolution of λ over time; (c): Predicted aging trajectories using conventional PF; and (d): Predicted aging trajectories using the proposed GC-PF.

cycles) for training is lower than the reference with the RMSE is greater than 2.5%.

Fourth, the effects of local behaviors can be reduced by using our proposed GC-PF method. Quantitatively, the RMSE of predictions are all limited within 1.86% for the above-mentioned three testing cases (FST2500, SONYVTC5 and FST2000). These improvements are mainly due to the global information within base model here is used in the entire training process, rather than only in the initialization stage. It can be seen that the testing profiles generally agree with the base models. In the light of this, λ in the (18) generally presents a value getting close to 1, as depicted in Fig. 2-(b) $\sim$ Fig. 4-(b). In this case, the optimization problem within (17) for gradient correction could be dominated

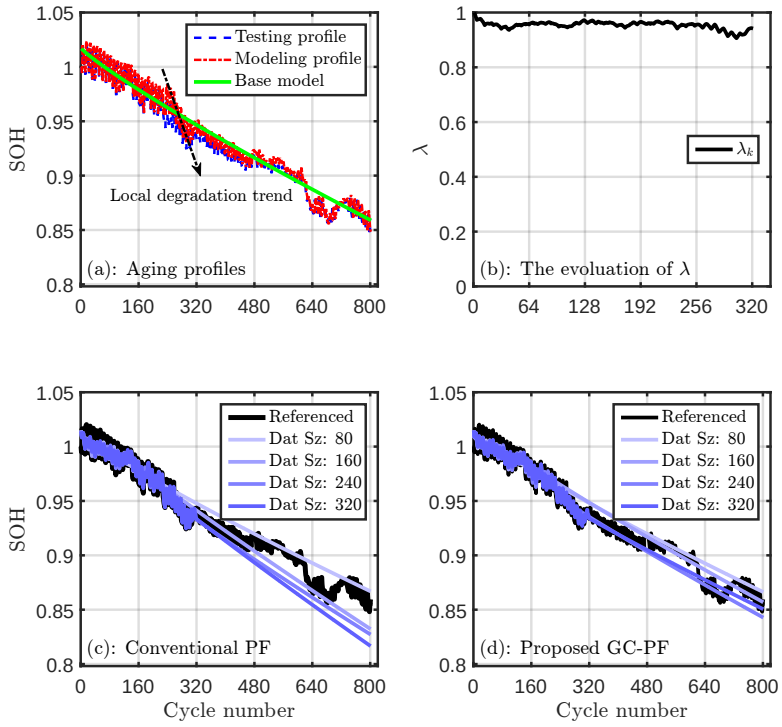

Figure 4: Experimental results using SONYVTC5 batteries. (a): Aging profiles of modeling and testing profiles; (b): The evolution of λ over time; (c): Predicted aging trajectories using conventional PF; and (d): Predicted aging trajectories using the proposed GC-PF.

by tracking the base model that provides the global battery aging behavior, and the effects of local behaviors within the aging trajectories would be reduced accordingly.

From the above observations, it is clear that the base model plays a vital role in the proposed GC-PF algorithm. Therefore, it is worthing to analyse the results under the case of there exists significant difference between the training and testing profiles. Here the widely used NASA battery data set is selected for verification purpose. As described in Table 1, the cut-off discharging voltages of the two cells are significantly different, resulting in the different aging trajectories as shown in Fig. 5-(a). For this scenario, the proposed GC-PF method still outperforms the conventional PF. Quantitatively, the RMSE of the proposed

method can be limited within 1.75% when using 40% of the data for training. The RMSE can be further reduced to 0.98% when 50% data is provided, and this result is 25% better than that of the conventional PF. In the proposed method, λ drops below 0.6 within 50 cycles, indicating that the influence of base model is reduced significantly. In such a case, the particle evolution is determined by both the PF part and a GC with reduced regularization term. Obviously, this GC-PF structure presents better results than just using conventional PF.

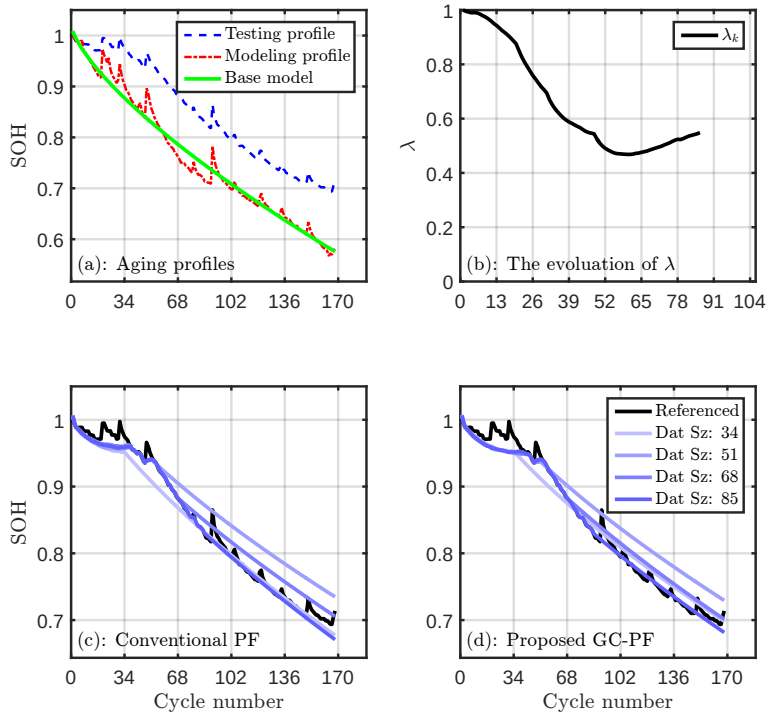

Figure 5: Experimental results using NASA batteries. (a): Aging profiles of modeling and testing profiles; (b): The evolution of λ over time; (c): Predicted aging trajectories using conventional PF; and (d): Predicted aging trajectories using the proposed GC-PF.

In addition to the RMSE, the MxAE values of prediction results for all algorithms are also evaluated. Quantitatively, the maximum MxAE of the proposed GC-PF is 6.05% for all batteries with different training data size, which is only 2.16% larger than that from the benchmark 2. Besides, when 40% (50%

for NASA data set) of total data is involved in training process, this MxAE performance can be even closer to the result of benchmark 2, with a difference limited by 1.30%. Due to the MxAE of benchmark 2 is the best result under the specific noise-polluted condition, in comparison with the MxAE difference between benchmark 1 and 2 (here is still 2.99% even if 40% data is involved in training phase), the relatively smaller MxAE difference (1.30%) indicates that the proposed GC-PF algorithm is able to achieve more accurate predictions.

Additionally, to evaluate the consistency of predictions under the conditions of different size of training data, a new criterion SDE is also utilized in this study. To emphasize the necessity of evaluating SDE, an numerical example using the results from Fig 3 is first provided. Specifically, when using conventional PF, the predicted SOH through training based on the first 10% of the aging data is 85.4% at cycle 400. However, under the condition of training model with 40% of the aging data, the predicted SOH at the 400th cycle becomes 81.3%, while SOH would be predicted to drop below 85.4% at the 317th cycle. Obviously, almost 25% difference on the battery lifetime prediction or 4.4% variation on the SOH prediction would occur when the starting point of prediction is different, which will significantly affect the users' confidence on the predicted battery lifetime. In the light of this, it is vital to adopt an effective criterion to evaluate the consistency of predictions. According to the SDE results in Table 5, it can be observed that the prediction consistency of GC-PF is better than those from benchmark 1 for all testing conditions (here is nearly 32% decrease). For the first three batteries, this improvement is mainly due to the fact that the accurate base model is utilized in the entire training process rather than just initialization. For the NASA battery data set, the reduced SDE is mainly caused by the improved tracking capability of GC-PF in comparison with the conventional PF.

5. Conclusions

Battery aging prediction exerts an enormously important role in the applications of power scheduling, energy management, thermal management etc.

This paper develops a hybrid approach through using a base model-oriented gradient-correction particle filter to predict the aging trajectory of Li-ion batteries. The main technical novelties arise from following aspects: First, through deriving a gradient-correction-particle filter, the tracking capability of PF can be improved. Second, through using the model-based regulation technique, the algorithm's sensitivity related to the local behavior of aging curve can be effectively reduced. In addition, apart from the commonly used RMSE and MxAE, a new criteria named SDE is also adopted to evaluate the consistency of prediction results. Through the extensive comparisons with other two benchmarks under extensive experimental tests of four types Li-ion cells, several quantitative results could be obtained as:

- When 40% aging data are used for model training that involves the measurement noise, the proposed GC-PF can achieve a high prediction accuracy (here the RMSE is less than 1.75%).
- With an effective base model, GC-PF is capable of providing a satisfactory prediction accuracy (here the RMSE is less than 1.86%) and a reduced training data down to 10%.
- In comparison with the results from benchmark 1, the SDE of the proposed algorithm presents 32% decrease, indicating a better consistency of predictions is achieved by using base model-oriented GC-PF algorithm.

To the best of our knowledge, this is the first known application by using model regularization technique with improved PF to handle battery aging trajectory prediction problem. The proposed algorithm could also be equally applicable to other battery aging predictions of energy management with appropriate data set.

Acknowledgement

This work was financially supported by National Natural Science Foundation of China project (61433005), Hong Kong Research Grant Council (16207717),

Guangdong Scientific and Technological Project (2017B010120002) and the European Union Horizon 2020 research and innovation programme (685716).

References

[1] H. He, R. Xiong, H. Guo, S. Li, Comparison study on the battery models used for the energy management of batteries in electric vehicles, Energy Conversion and Management 64 (2012) 113–121.

[2] H. Liu, Z. Wei, W. He, J. Zhao, Thermal issues about li-ion batteries and recent progress in battery thermal management systems: A review, Energy conversion and management 150 (2017) 304–330.

[3] K. Liu, C. Zou, K. Li, T. Wik, Charging pattern optimization for lithium-ion batteries with an electrothermal-aging model, IEEE Transactions on Industrial Informatics 14 (12) (2018) 5463–5474.

[4] X. Tang, C. Zou, T. Wik, K. Yao, Y. Xia, Y. Wang, D. Yang, F. Gao, Run-to-run control for active balancing of lithium iron phosphate battery packs, IEEE Transactions on Power Electronics.

[5] K. Liu, X. Hu, Z. Yang, Y. Xie, S. Feng, Lithium-ion battery charging management considering economic costs of electrical energy loss and battery degradation, Energy Conversion and Management 195 (2019) 167–179.

[6] R. Xiong, L. Li, J. Tian, Towards a smarter battery management system: A critical review on battery state of health monitoring methods, Journal of Power Sources 405 (2018) 18–29.

[7] M. Berecibar, I. Gandiaga, I. Villarreal, N. Omar, J. Van Mierlo, P. Van den Bossche, Critical review of state of health estimation methods of Li-ion batteries for real applications, Renewable and Sustainable Energy Reviews 56 (2016) 572–587.

[8] F. Feng, X. Hu, L. Hu, F. Hu, Y. Li, L. Zhang, Propagation mechanisms and diagnosis of parameter inconsistency within li-ion battery packs, Renewable and Sustainable Energy Reviews 112 (2019) 102 – 113.

[9] S. M. Rezvanizaniani, Z. Liu, Y. Chen, J. Lee, Review and recent advances in battery health monitoring and prognostics technologies for electric vehicle (EV) safety and mobility, Journal of Power Sources 256 (2014) 110–124.

[10] Y. Liu, J. Li, Z. Chen, D. Qin, Y. Zhang, Research on a multi-objective hierarchical prediction energy management strategy for range extended fuel cell vehicles, Journal of Power Sources 429 (2019) 55 – 66.

[11] K. Liu, K. Li, Q. Peng, C. Zhang, A brief review on key technologies in the battery management system of electric vehicles, Frontiers of Mechanical Engineering 14 (1) (2019) 47–64.

[12] L. Kang, X. Zhao, J. Ma, A new neural network model for the state-of-charge estimation in the battery degradation process, Applied Energy 121 (2014) 20–27.

[13] M. De Smith, Statsref: Statistical analysis handbook-a web-based statistics resource (2015).

[14] A. Eddahech, O. Briat, N. Bertrand, J.-Y. Deletage, J.-M. Vinassa, Behavior and state-of-health monitoring of Li-ion batteries using impedance spectroscopy and recurrent neural networks, International Journal of Electrical Power & Energy Systems 42 (1) (2012) 487–494.

[15] A. Nuhic, T. Terzimehic, T. Soczka-Guth, M. Buchholz, K. Dietmayer, Health diagnosis and remaining useful life prognostics of lithium-ion batteries using data-driven methods, Journal of power sources 239 (2013) 680–688.

[16] D. Liu, J. Zhou, H. Liao, Y. Peng, X. Peng, A health indicator extraction and optimization framework for lithium-ion battery degradation modeling

and prognostics, IEEE Transactions on Systems, Man, and Cybernetics: Systems 45 (6) (2015) 915–928.

[17] J. Luo, M. Namburu, K. Pattipati, L. Qiao, M. Kawamoto, S. Chigusa, Model-based prognostic techniques [maintenance applications], in: Proceedings AUTOTESTCON 2003. IEEE Systems Readiness Technology Conference., IEEE, 2003, pp. 330–340.

[18] C. Lyu, Q. Lai, T. Ge, H. Yu, L. Wang, N. Ma, A lead-acid battery's remaining useful life prediction by using electrochemical model in the particle filtering framework, Energy 120 (2017) 975–984.

[19] L. Liao, F. Köttig, Review of hybrid prognostics approaches for remaining useful life prediction of engineered systems, and an application to battery life prediction, IEEE Transactions on Reliability 63 (1) (2014) 191–207.

[20] L. Zhang, Z. Mu, C. Sun, Remaining useful life prediction for lithium-ion batteries based on exponential model and particle filter, IEEE Access 6 (2018) 17729–17740.

[21] W. He, N. Williard, M. Osterman, M. Pecht, Prognostics of lithium-ion batteries based on dempster–shafer theory and the bayesian monte carlo method, Journal of Power Sources 196 (23) (2011) 10314–10321.

[22] C. Hu, H. Ye, G. Jain, C. Schmidt, Remaining useful life assessment of lithium-ion batteries in implantable medical devices, Journal of Power Sources 375 (2018) 118–130.

[23] Y. Sun, X. Hao, M. Pecht, Y. Zhou, Remaining useful life prediction for lithium-ion batteries based on an integrated health indicator, Microelectronics Reliability 88 (2018) 1189–1194.

[24] M. Zeitz, The extended luenberger observer for nonlinear systems, Systems & Control Letters 9 (2) (1987) 149–156.

[25] R. K. Singleton, E. G. Strangas, S. Aviyente, Extended kalman filtering for remaining-useful-life estimation of bearings, IEEE Transactions on Industrial Electronics 62 (3) (2014) 1781–1790.

[26] J. Wei, G. Dong, Z. Chen, Remaining useful life prediction and state of health diagnosis for lithium-ion batteries using particle filter and support vector regression, IEEE Transactions on Industrial Electronics 65 (7) (2017) 5634–5643.

[27] M. S. Arulampalam, S. Maskell, N. Gordon, T. Clapp, A tutorial on particle filters for online nonlinear/non-gaussian bayesian tracking, IEEE Transactions on signal processing 50 (2) (2002) 174–188.

[28] X. Tang, Y. Wang, C. Zou, K. Yao, Y. Xia, F. Gao, A novel framework for lithium-ion battery modeling considering uncertainties of temperature and aging, Energy Conversion and Management 180 (2019) 162–170.

[29] R. Xiong, Q. Yu, W. Shen, C. Lin, F. Sun, A sensor fault diagnosis method for a lithium-ion battery pack in electric vehicles, IEEE Transactions on Power Electronics PP (99) (2019) 1–1.

[30] Y. Wang, C. Zhang, Z. Chen, A method for state-of-charge estimation of lifepo4 batteries at dynamic currents and temperatures using particle filter, Journal of power sources 279 (2015) 306–311.

[31] M. Lewerenz, J. Münnix, J. Schmalstieg, S. Käbitz, M. Knips, D. U. Sauer, Systematic aging of commercial lifepo4— graphite cylindrical cells including a theory explaining rise of capacity during aging, Journal of Power Sources 345 (2017) 254–263.

[32] B. Saha, K. Goebel, Battery data set, NASA AMES prognostics data repository PP (99) (2007) 1–1.

[33] X. Tang, C. Zou, K. Yao, G. Chen, B. Liu, Z. He, F. Gao, A fast estimation algorithm for lithium-ion battery state of health, Journal of Power Sources 396 (2018) 453–458.

[34] X. Tang, K. Yao, B. Liu, W. Hu, F. Gao, Long-term battery voltage, power, and surface temperature prediction using a model-based extreme learning machine, Energies 11 (1) (2018) 86.

[35] K. Liu, K. Li, H. Ma, J. Zhang, Q. Peng, Multi-objective optimization of charging patterns for lithium-ion battery management, Energy Conversion and Management 159 (2018) 151–162.

[36] K. Liu, K. Li, Z. Yang, C. Zhang, J. Deng, An advanced lithium-ion battery optimal charging strategy based on a coupled thermoelectric model, Electrochimica Acta 225 (2017) 330–344.

[37] M. Lucu, E. Martinez-Laserna, I. Gandiaga, H. Camblong, A critical review on self-adaptive Li-ion battery ageing models, Journal of Power Sources 401 (2018) 85–101.

[38] Y. Li, K. Liu, A. M. Foley, A. Zulke, Data-driven health estimation and lifetime prediction of lithium-ion batteries: a review, Renewable and Sustainable Energy Reviews, 2019, accepted.

[39] D. Wang, Q. Miao, M. Pecht, Prognostics of lithium-ion batteries based on relevance vectors and a conditional three-parameter capacity degradation model, Journal of Power Sources 239 (2013) 253–264.

[40] J. Carpenter, P. Clifford, P. Fearnhead, Improved particle filter for nonlinear problems, IEE Proceedings-Radar, Sonar and Navigation 146 (1) (1999) 2–7.

[41] M. A. Kouritzin, Residual and stratified branching particle filters, Computational Statistics & Data Analysis 111 (2017) 145–165.

[42] S. Ruder, An overview of gradient descent optimization algorithms, arXiv preprint arXiv:1609.04747.

[43] D. W. Marquardt, An algorithm for least-squares estimation of nonlinear parameters, Journal of the society for Industrial and Applied Mathematics 11 (2) (1963) 431–441.

[44] K. Liu, K. Li, Q. Peng, Y. Guo, L. Zhang, Data-driven hybrid internal temperature estimation approach for battery thermal management, Complexity 2018.